Chapter 3
Turning Dynamics

Make everything as simple as possible, but not simpler.

– Albert Einstein

In Chapter 2, we discussed how to use modal analysis to describe the tool point dynamics for tool-holder combinations. In this chapter, we'll discuss regenerative chatter in turning and see how we can apply the dynamics information to develop stability lobe diagrams that describe the limiting chip width (to avoid chatter) as a function of spindle speed. We'll also detail a time-domain simulation for predicting cutting force and tool displacement which also enables us to determine stable and unstable cutting conditions.

3.1 Turning Description

Turning operations are generally carried out on a lathe where a workpiece is rotated in a spindle past a tool mounted on a two axis slide in order to give the desired shape to the axisymmetric part; see Fig. 3.1.1. The final shape can include both internal and external features. The lathe may be manual, where a machinist controls the slide positions during material removal, or computer numerically controlled (CNC). In this case, automatic control is used to command the slide positions to follow the path described by the part program. The part program is based on the desired workpiece dimensions and is typically developed using computer aided design/computer aided manufacturing (CAD/CAM) software.

During turning, a sharp cutting edge is used to remove material in the form of a chip. Many studies have been performed to better understand chip formation and the associated mechanics, but our focus is a broader view of the resulting cutting force and corresponding vibrations of the tool. Therefore, we will not focus so much on the chip itself as on the corresponding system behavior. Texts that provide more information regarding metal cutting
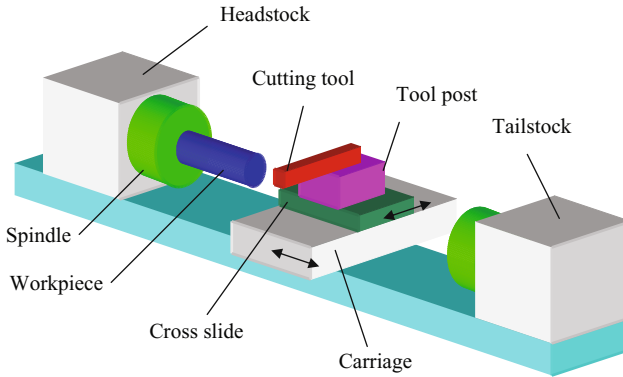
Fig. 3.1.1 Schematic of manual lathe. The workpiece is clamped in the rotating spindle, but may also be supported at its free end using the tailstock. The cutting tool, which is clamped to the tool post, is moved relative to the workpiece by adjusting the positions of the carriage (axial direction) and cross slide (radial direction)

fundamentals, heat generation and heat transfer during cutting, and related technology include, for example, [1–4].

To begin, let's consider the tool and workpiece to be rigid and develop expressions for the cutting force, F. Figure 3.1.2 shows an "orthogonal cutting" operation, where only the normal, F_n, and tangential, F_t, components of the force are considered. In general, the cutting force vector includes the third component along the part axis, but the orthogonal treatment is sufficient for us to describe the process dynamics. The figure also identifies: 1) the mean chip thickness, h_m, or commanded feed per revolution for the facing operation pictured; and 2) the force angle, β, between F and F_n. The side view of this operation (inset in Fig. 3.1.2) shows the chip width, b. Together, the chip
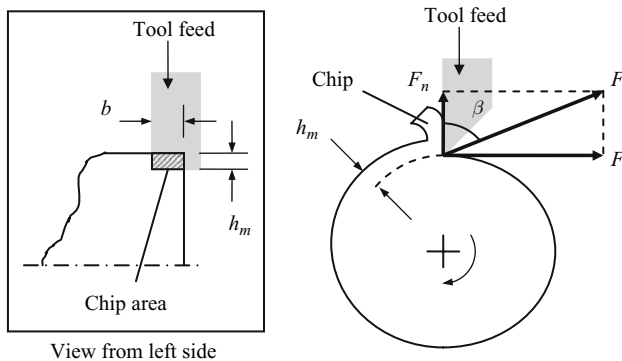

Fig. 3.1.2 Orthogonal cutting operation showing the cutting force with its normal and tangential components

thickness and chip width define the area of material to be removed, $A = bh_m$. We approximate the cutting force as the product of this chip area and an empirical coefficient. This process dependent coefficient is referred to as the specific (or per unit chip area) force, K_s, in [2] and depends on the workpiece material, tool geometry, and, to a lesser extent, the cutting speed (peripheral velocity of the rotating workpiece) and chip thickness.

$$F = K_s A = K_s bh_m \tag{3.1.1}$$

The normal and tangential components, F_n and F_t, can be expressed using F and the force angle:

$$F_n = \cos(\beta)F = \cos(\beta)K_s bh_m = k_n bh_m \text{ and} \tag{3.1.2}$$

$$F_t = \sin(\beta)F = \sin(\beta)K_s bh_m = k_t bh_m, \tag{3.1.3}$$

where we've defined the cutting force coefficients, k_n and k_t, which incorporate both K_s and β. Although efforts continue to calculate these coefficients based on elastic and plastic material properties, a common approach used to characterize these process dependent values is to prescribe known cutting conditions and measure the force components directly. If the tool is mounted on a cutting force dynamometer as shown in Fig. 3.1.3 and the b and h_m values are known, then the measured force component values can be used to determine the coefficients by rewriting Eqs. 3.1.2 and 3.1.3, $k_n = \frac{F_n}{bh_m}$ and $k_t = \frac{F_t}{bh_m}$. Typical units for k_n, k_t, and K_s are N/mm^2.
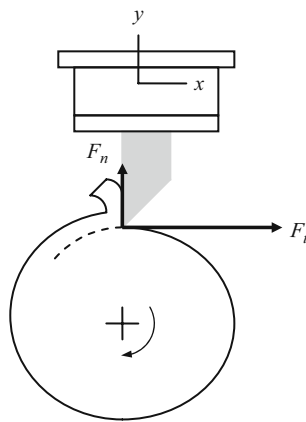

Fig. 3.1.3 Force measurement during turning using a cutting force dynamometer. The tangential and normal cutting forces are measured as the x and y dynamometer force components

Table 3.1.1 Representative K_s values for selected workpiece materials [2]

Material	K_s (N/mm^2)	Material	K_s (N/mm^2)
Gray cast iron	1500	Ni-based Inconel X	3400
1020 carbon steel	2100	Ni-based Udimet 500	3500
1035 carbon steel	2300	Co-based L605	3500
1045 carbon steel	2600	Ti (6Al, 4 V)	2000
302 stainless steel	2700	Al 7075-T6	850
4140/5140 alloy steel	2800	Al 6061-T6	750

Selected K_s values are provided in [2, Tables 7.1 and 8.1]. These have been reproduced in Table 3.1.1, but should be considered to be representative values and not necessarily specific to a particular application.

IN A NUTSHELL   The force produced by the cutting opera-tion is proportional to the frontal area of the chip through the coefficient K_s. Deriving K_s from first principles is quite difficult and, in this way, it is similar to the elastic modulus, E. Tabulated values are approximate and often good enough. High precision applications, on the other hand, may require careful measurement of the cut geometry and resulting forces using the intended tooling and workpiece mate-rials, F.

3.2 Regenerative Chatter in Turning

If we remove the assumption of a rigid tool, then it is clear that the cutting force will cause deflections of the cutting tool. Because the tool has stiffness and mass, it can vibrate. If the tool is vibrating as it removes material, these vibrations are imprinted on the workpiece surface as a wavy profile. Figure 3.2.1 shows an exaggerated view, where the initial impact with the workpiece surface causes the tool to begin vibrating and the oscillations in the normal direction to be copied onto the workpiece. When the workpiece begins its second revolution, the vibrating tool encounters the wavy surface produced during the first revolution. Therefore, the chip thickness at any instant depends both on the tool deflection at that time and the workpiece surface from the previous revolution. Vibration of the tool therefore leads to a variable chip thickness which, according to Eq. 3.1.1, will give a variable cutting force since the force is proportional to the chip thickness. The cutting force governs the current tool deflection and, subsequently, the system exhibits feedback. In other words, the current behavior depends on previous behavior – the system has a "memory".
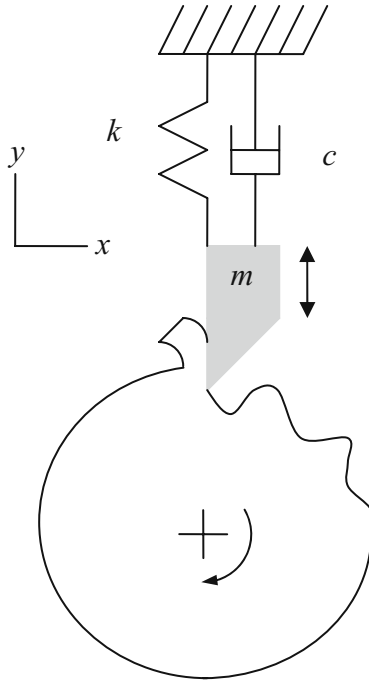
Fig. 3.2.1 Description of regenerative chatter in turning. Initial tool deflections are copied onto the workpiece surface and are encountered in subsequent revolutions. This varies the chip thickness and cutting force which, in turn, affects the resulting tool deflections

IN A NUTSHELL   Cutting produces a force that is proportional to the chip thickness and chip width. While the tool is stiff in comparison to objects in our everyday lives, it is not infinitely stiff. For this reason, varying cutting forces (from transients such as the initial contact of the tool with the workpiece) produce vibrations of the tool. The vibrating tool changes the chip thickness and leaves a wavy surface. Variable forces cause vibrations... vibrations cause wavy surfaces...wavy surfaces produce variable forces. The reality is that the cutting operation is only partially governed by the selected geometry. Dynamics, the response of a flexible system to varying forces, plays a strikingly powerful role.

From a modeling standpoint, this "regeneration of waviness" appears as a time-delayed term in the chip thickness equation. Figure 3.2.2 shows an unwrapped view of the turning operation, where the surface on the left was produced in the previous revolution and the surface to the right of the tool (offset by the mean feed per revolution) was just cut away by the oscillating tool.
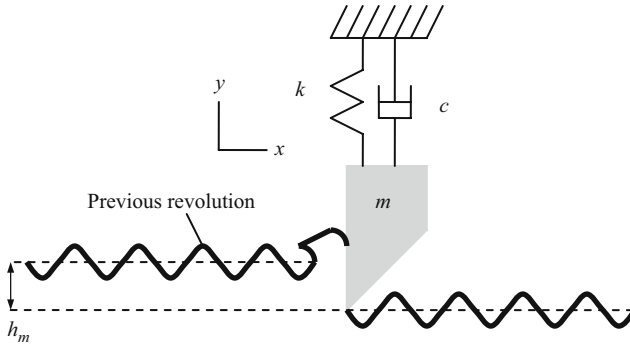
Fig. 3.2.2 Depiction of turning where the surface from the previous revolution, shown to the left of the tool, is removed by the vibrating cutter to produce a new wavy surface to the right of the tool

We will consider only vibrations in the normal direction, y (positive direction out of the cut), which has the most direct influence on the chip thickness.

The time dependent, instantaneous chip thickness, $h(t)$, is determined using Eq. 3.2.1. It is seen that larger positive vibration during the previous revolution, $y(t - \tau)$, where τ is the time for one rotation, gives an increased chip thickness (i.e., less material was removed so the current chip is thicker). Larger positive current vibration, $y(t)$, on the other hand, yields a thinner chip. See Fig. 3.2.3.

$$h(t) = h_m + y(t - \tau) - y(t) \tag{3.2.1}$$

The relative phasing between the surface waviness from one pass to the next determines the level of force variation and whether the operation is stable or
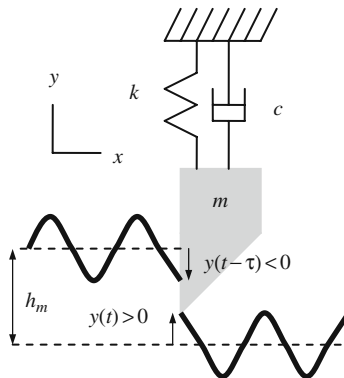

Fig. 3.2.3 The figure demonstrates the instantaneous chip thickness calculation. It depends on the mean feed per revolution, the current deflection, and the vibration during the previous revolution of the workpiece (to the left of the tool)
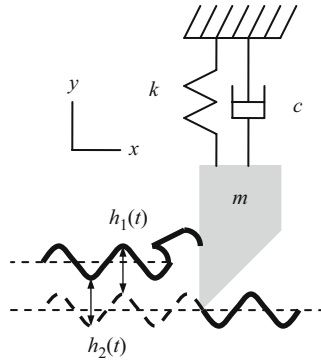
Fig. 3.2.4 The surface waviness between revolutions is in phase. Negligible chip thickness variation is obtained
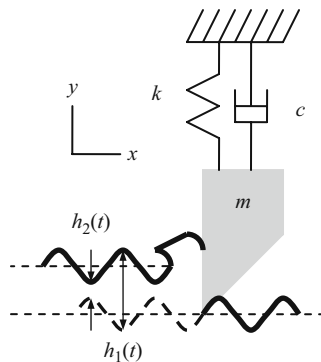

Fig. 3.2.5 Less favorable phase relationship between revolutions yields significant chip thickness variation

unstable (chatter occurs). Figures 3.2.4 and 3.2.5 show two possibilities. In Fig. 3.2.4, the wavy surfaces between two revolutions are in phase. Therefore, even though vibration is present during material removal, the chip thickness variation (vertical distance between the two curves) is negligible and there is no appreciable force variation. This enables stable cutting at larger chip widths. Considering that the tool tends to vibrate at its natural frequency, it is intuitive that matching the workpiece rotating frequency (spindle speed) to the tool's natural frequency will lead to this preferred "in phase" situation. However, this is counter intuitive based on our traditional understanding of resonance where we avoid driving the system at its natural frequency. Figure 3.2.5 shows a less favorable phase relationship where there is significant variation in the chip thickness. This leads to unstable cutting at smaller chip widths than the previous case due to the force variations and subsequent tool deflections.

IN A NUTSHELL   The cutting force is very sensitive to the revolution-to-revolution alignment of the current tool motion to the previous motion of the tool imprinted on the surface. A "good" alignment (in phase) results in negligible chip thickness variation. A "bad" alignment (180 deg out of phase) produces a strong chip thickness variation. The worst case occurs when significant variation in the chip thickness coincides with a large magnitude in the frequency response function. It turns out that the worst case is about 270 deg out of phase.

3.3 Stability Lobe Diagrams

Depending on the feedback system "gain", or chip width b, and spindle speed, Ω, the turning operation will either be stable or exhibit chatter (unstable cutting), which causes large vibrations and forces and leads to poor surface finish and, potentially, tool/workpiece damage. In stable machining, the vibrations diminish from revolution to revolution. In unstable machining, the vibrations grow from revolution to revolution until limited in some way. Surprisingly, the vibrations may become large enough that the tool jumps out of the cut, losing contact with the workpiece. The vibrations in unstable cutting may be at least as large as the chip thickness and it is not surprising these large vibrations may result in damage to the machine, tool, and workpiece. The governing relationships for this behavior are provided in Eqs. 3.3.1 through 3.3.3 [2].

$$b_{\lim} = \frac{-1}{2K_s \cos(\beta) \mathrm{Re}[FRF]} \tag{3.3.1}$$

$$\frac{f_c}{\Omega} = N + \frac{\varepsilon}{2\pi} \tag{3.3.2}$$

$$\varepsilon = 2\pi - 2\tan^{-1}\left(\frac{\mathrm{Re}[FRF]}{\mathrm{Im}[FRF]}\right) \tag{3.3.3}$$

In these equations, $b_{\lim}$ is the limiting chip width to avoid chatter, f_c is the chatter frequency (should it occur), N is the integer number of waves of vibration imprinted on the workpiece surface in one revolution, and $\frac{\varepsilon}{2\pi}$ is any additional fraction of a wave, where ε is the phase (in rad) between current and previous tool vibrations. Note that for units consistency in Eq. 3.3.2, if f_c is expressed in Hz, then Ω must be specified in rev/s. Figure 3.3.1 shows an example stability lobe diagram where the Ω versus $b_{\lim}$ family of curves ($N = 0, 1, 2, \ldots$) separate the space into two regions. Any (Ω, $b_{\lim}$) pair that appears above the collective boundary indicates unstable behavior, while any pair below the boundary is presumed to be stable. We'll next discuss the foundation of the
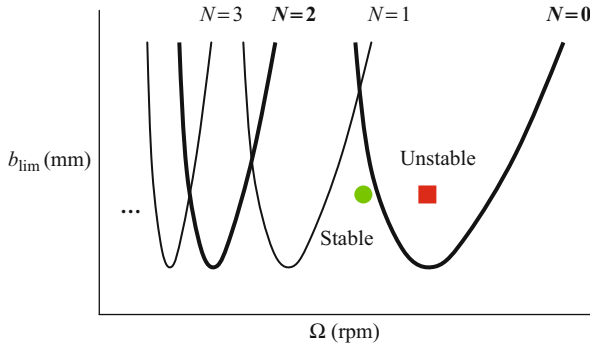
Fig. 3.3.1 Example stability lobe diagram. The stability boundary separates stable chip width-spindle speed combinations (below the boundary, marked as a circle) from unstable pairs (above, marked as a square)

relationships, provided in Eqs. 3.3.1 through 3.3.3, that are applied to construct this diagram. We'll base this discussion on the normal force equation and the vector representation of tool deflections in the complex plane.

IN A NUTSHELL   Whether we know it or not, whether we like it or not, every cutting operation has a picture like the one shown in Fig. 3.3.1. If we choose the cutting conditions at random, or at least without considering the applicable stability lobe diagram, then we sometimes choose stable cutting and sometimes not. Sometimes speeding up helps and other times it makes things worse. It appears to be random and many machine shops struggle with this issue every day. If we have the diagram and choose the cutting conditions accordingly, then it is possible to avoid the unstable conditions (chatter) and increase productivity.

Equation 3.2.1 shows that the instantaneous chip thickness depends on the commanded chip thickness, the normal direction vibration one revolution earlier, and the current vibration in the normal direction. If we substitute this $h(t)$ for h_m in the normal force expression provided in Eq. 3.1.2, we obtain:

$$F_n = k_n b h(t) = k_n b(h_m + y(t - \tau) - y(t)). \qquad (3.3.4)$$

This force equation has both a constant part, $k_n b h_m$, and a variable part, $k_n b(y(t - \tau) - y(t))$. The constant part does not influence the stability of the linear system. We are therefore interested in the behavior of the variable part. To explore the value of b as a function of k_n and the tool vibrations, let's consider a unit value of the variable force, or $1 = k_n b(y(t - \tau) - y(t))$ from Eq. 3.3.4. This equation can be solved for b:

$$b = \frac{1}{k_n(y(t-\tau) - y(t))}. \qquad (3.3.5)$$

Regarding the vibration levels from one revolution to the next in Eq. 3.3.5, we can state the following:

- if $y(t) > y(t-\tau)$, then the vibrations are growing from one revolution to the next and unstable behavior results;
- $y(t) = y(t-\tau)$ indicates the limit of stability – the vibration level is neither increasing or decreasing; and
- $y(t) < y(t-\tau)$, then the vibrations are decaying from one revolution to the next and stable behavior is achieved.

Let's draw the $\vec{y}(t)$ and $\vec{y}(t-\tau)$ vectors in the complex plane for the limiting case that $\vec{y}(t) = \vec{y}(t-\tau)$[1]. We will require that the following vector sum is satisfied:

$$\vec{y} + (\vec{y}(t-\tau) - \vec{y}) = \vec{y}(t-\tau). \qquad (3.3.6)$$

It is also necessary that the difference $\vec{y}(t-\tau) - \vec{y}(t)$, which represents the variable part of the chip thickness, is real valued. In other words, the instantaneous chip thickness is a scalar quantity; it has no imaginary part. In the complex plane it must therefore be horizontal. Figure 3.3.2 shows the vectors $\vec{y}(t)$ and $\vec{y}(t-\tau)$ as well as the real valued difference $\vec{y}(t-\tau) - \vec{y}(t)$ for a single degree of freedom system. Note the similarity to Fig. 2.2.6. The real valued unit
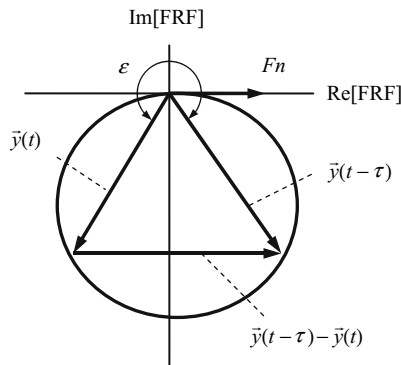

Fig. 3.3.2 Vector representation of unit normal force and tool deflections (current and previous revolutions) for limit of stability

---

[1] We represent $\vec{y}(t)$ and $\vec{y}(t-\tau)$ as vectors because they have both a magnitude and phase relative to the force, F_n. The force and both displacement vectors are displayed in Fig. 3.3.2.
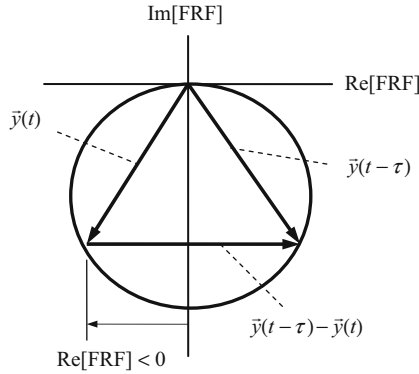
Fig. 3.3.3 Representing the length of the vector difference using the negative real part of the tool point FRF

normal force and the phase between tool vibrations in subsequent revolutions, ε, are also shown. The geometry seen in this figure satisfies the following requirements: 1) the magnitude and phase of the tool deflections depend on the forcing frequency (spindle speed) and the tool's direct FRF as measured at the cutting edge; 2) the amplitudes for $\vec{y}(t)$ and $\vec{y}(t - \tau)$ are equal (limit of stability); and 3) the difference $\vec{y}(t - \tau) - \vec{y}(t)$ is horizontal.

We can now rewrite Eq. 3.3.5 by substituting for $\vec{y}(t - \tau) - \vec{y}(t)$. Figure 3.3.3 shows that, due to the approximate symmetry, the length of the vector difference can be written as twice the negative real (Re) part of the tool's direct FRF. Equation 3.3.7 shows the new relationship, where the negative sign is included in order to obtain positive (limiting) chip width values. This equation matches Eq. 3.3.1, where k_n is substituted for the product $K_s \cos(\beta)$:

$$b_{\lim} = \frac{-1}{k_n(2\mathrm{Re}[FRF])}. \qquad (3.3.7)$$

IN A NUTSHELL   It is the chip width (and not the chip thickness) that controls whether or not the cutting operation is stable. The real part of the frequency response function defines the limiting chip width. The higher the system's dynamic stiffness (more stiffness and more damping), the larger the chip width that can be obtained without chatter.

Given Eq. 3.3.7, we can determine the smallest and largest potential values of $b_{\lim}$ based on the range of magnitudes possible for the negative real part of the tool point FRF. The smallest value is obtained for the minimum, or most negative, value of Re[FRF], when the absolute value of the denominator is

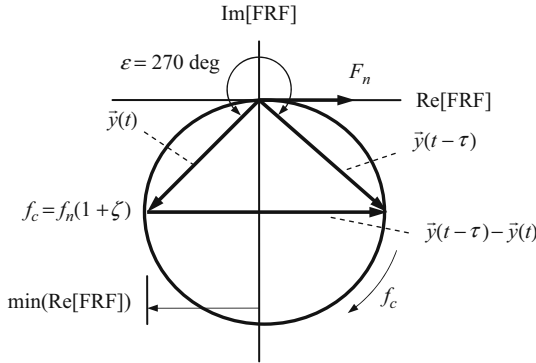**Fig. 3.3.4** Vector representation of $b_{\text{lim,crit}}$ case ($f_c = f_n(1 + \zeta)$ and $\varepsilon = 270$ deg)

largest. We will refer to this minimum b_{lim} value as the critical value, $b_{\text{lim,crit}}$. See Eq. 3.3.8. The chatter frequency for this case (i.e., the min(Re[FRF])) is $f_c = f_n(1 + \zeta)$ as shown in Fig. 2.2.5. The situation is pictured in Fig. 3.3.4. From the figure, we also see that ε is $\frac{3\pi}{2}$ rad or 270 deg. A representation of the time dependent tool deflections with this phase relationship is shown in Fig. 3.3.5. Again, the chip thickness variation is determined from the vertical distance between the two curves. It is interesting to note that the worst case (smallest chip width) is not obtained when $\varepsilon = 180$ deg, or the vibrations from one revolution to the next are exactly out of phase.

$$b_{\text{lim,crit}} = \frac{-1}{k_n(2 \cdot \min(\text{Re}[FRF]))} \quad (3.3.8)$$

The largest b_{lim} value is obtained when $\varepsilon = 360$ deg. This is the "in phase" situation of negligible chip thickness variation. As seen in the complex plane representation given in Fig. 3.3.6, the real part of the tool point FRF is zero and the chatter frequency is f_n. Substitution in Eq. 3.3.7 would suggest an infinite chip thickness, $b_{\text{lim}} = \frac{-1}{k_n(2 \cdot 0)} = \infty$. However, we obtain finite b_{lim} values for the
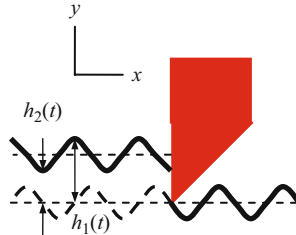

Fig. 3.3.5 Chip thickness variation for the $b_{\text{lim,crit}}$ case when $\varepsilon = 270$ deg
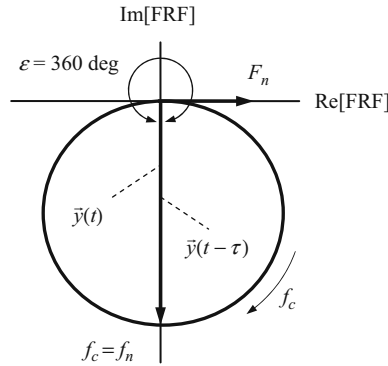
Fig. 3.3.6 Vector representation of largest $b_{\lim}$ case with favorable phase relationship ($\varepsilon = 360$ deg) between subsequent workpiece revolutions

left end of the $N = 0$ curve, even at a chatter frequency equal to f_n, because the adjacent stability curve with one more wave per revolution ($N = 1$) intersects the original curve and truncates it. See Fig. 3.3.7.

We see a similar situation as the chatter frequency approaches infinity, $f_c \rightarrow \infty$. In this case (Fig. 3.3.8), even though the revolution to revolution phase relationship is unfavorable ($\varepsilon \rightarrow 180°$, deg, or exactly out of phase), the response amplitude approaches zero, $\text{Re}(FRF) \rightarrow 0$.. Again, substitution in Eq. 3.3.7 would suggest an infinite chip thickness, $b_{\lim} = \frac{-1}{k_n(2 \cdot 0)} = \infty$. However, as seen in Fig. 3.3.7, the left side of the $N = 0$ curve serves to limit the right hand side of the $N = 1$ curve where $f_c \rightarrow \infty$.

We'll now see how each individual stability curve is actually a mapping of $\text{Re}[FRF]$ onto the $(\Omega, b_{\lim})$ diagram. We'll first consider the $N = 0$ curve, which
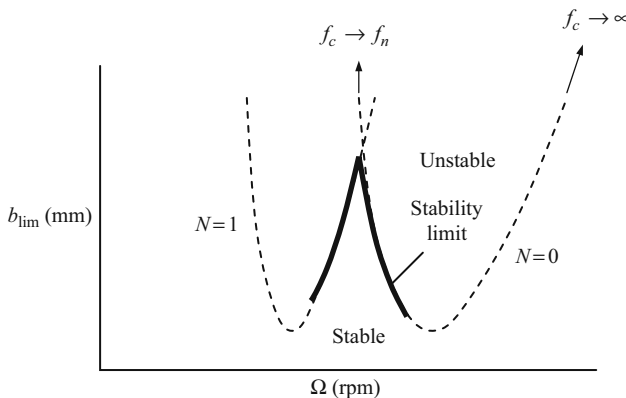

Fig. 3.3.7 Stability lobe diagram exhibiting truncation of $N = 0$ stability curve by $N = 1$ curve to obtain finite $b_{\lim}$ values
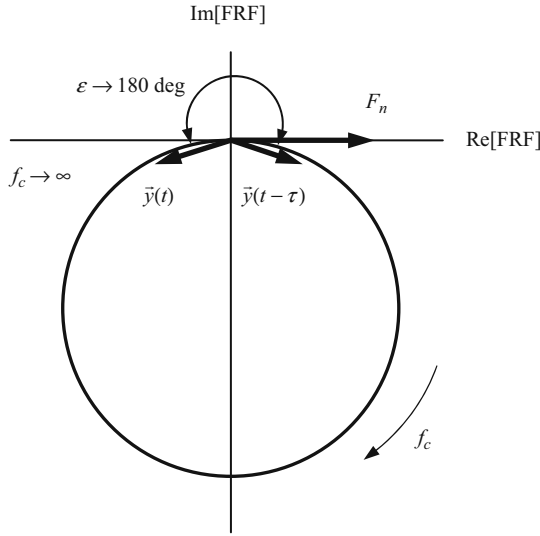
Fig. 3.3.8 Vector representation of $\varepsilon = 180$ deg phase relationship between subsequent workpiece revolutions ($f_c \to \infty$)

means that less than one wave is imprinted on the surface per revolution. We've already discussed the $b_{\lim}$ values, so we'll now focus on the spindle speeds for the left end (labeled as 1 in Fig. 3.3.9), the minimum (2), and the right end (3). As we saw in Fig. 3.3.6, when the chatter frequency is equal to f_n, the $\varepsilon = 360$ deg $= 2\pi$ rad phase relationship is obtained and $b_{\lim} = \infty$ because the real part is zero. Point 1 therefore has a spindle speed of:
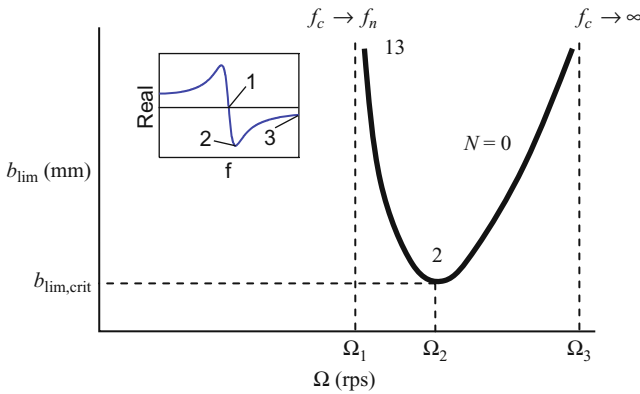

Fig. 3.3.9 Mapping of the real part of the tool point FRF onto the (Ω, $b_{\lim}$) diagram for the $N = 0$ lobe. Spindle speeds provided in Eqs. 3.3.9 through 3.3.11

$$\Omega_1 = \frac{f_c}{N + \frac{\varepsilon}{2\pi}} = \frac{f_n}{0 + \frac{2\pi}{2\pi}} = f_n \tag{3.3.9}$$

from Eq. 3.3.2. (Note that units of Hz for f_n gives equivalent units of rev/s, or rps, for spindle speed.) This corresponds to point 1 in the inset showing the real part of the tool point FRF.

IN A NUTSHELL   The chip width can be very large without the occurrence of chatter if the spindle speed is set close to the natural frequency of the most flexible vibration mode. This surprising result comes from favorable alignment of the waviness from one revolution to the next at this speed.

Recall that we are only considering the negative portion of the real part so the applicable frequency range (for this single degree of freedom response) is f_n to ∞. At point 2, which has the minimum chip width, $b_{\text{lim,crit}}$, we saw in Fig. 3.3.4 that the chatter frequency is $f_n(1 + \zeta)$ and $\varepsilon = 270 \deg = \frac{3\pi}{2}$ rad. The corresponding spindle speed is:

$$\Omega_2 = \frac{f_n(1 + \zeta)}{0 + \frac{3\pi}{2}{2\pi}} = \frac{4}{3}f_n(1 + \zeta) \tag{3.3.10}$$

At point 3 the chatter frequency approaches ∞ and ε approaches $180 \deg = \pi$ rad. rad. The spindle speed is:

$$\Omega_3 = \frac{\infty}{0 + \frac{\pi}{2\pi}} = \infty. \tag{3.3.11}$$

Let's next consider the $N = 1$ stability curve (or lobe). In this case, there is at least one wave of vibration per revolution. See Fig. 3.3.10. Although the b_{lim} values are a function of the chatter frequency (via the tool point FRF), they do not depend on the lobe number, N. Therefore, these values do not change relative to the $N = 0$ calculations. Similarly, the ε values are independent of the lobe number and do not change. The spindle speed equation (Eq. 3.3.2), however, is a function of the lobe number. Using the same labeling convention for the left end, minimum, and right end points of Re[FRF], we obtain the three spindle speeds:

$$\Omega_1 = \frac{f_n}{1 + \frac{2\pi}{2\pi}} = \frac{f_n}{2}, \tag{3.3.12}$$

$$\Omega_2 = \frac{f_n(1 + \zeta)}{1 + \frac{3\pi}{2}{2\pi}} = \frac{4}{7}f_n(1 + \zeta), \text{ and} \tag{3.3.13}$$
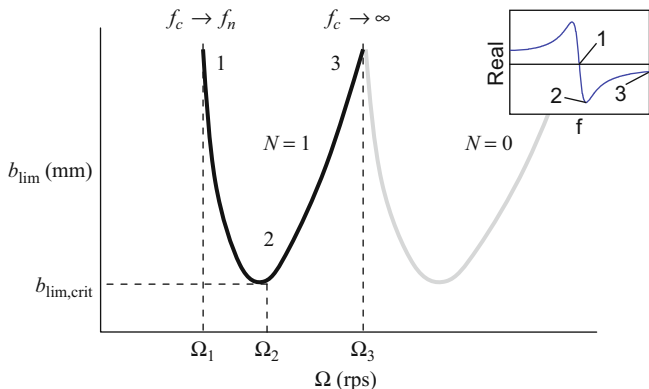
Fig. 3.3.10 Mapping of the real part of the tool point FRF onto the $(\Omega, b_{\lim})$ diagram for the $N = 1$ lobe. Spindle speeds provided in Eqs. 3.3.12 through 3.3.14

$$\Omega_3 = \frac{\infty}{1 + \frac{\pi}{2\pi}} = \infty. \tag{3.3.14}$$

If we plot multiple lobes ($N = 0, 1, 2, \ldots$), we obtain a result similar to Fig. 3.3.11. We see that all lobes exhibit the same minimum value, $b_{\lim,crit}$, and the peak values are located approximately at integer fractions of the tool point natural frequency. We can therefore write a "best speeds" equation which identifies these spindle speeds (in rev/min, or rpm). See Eq. 3.3.15, where f_n is expressed in Hz. As noted, any $(\Omega, b_{\lim})$ pair located below the stability boundary leads to stable operation, while combinations above the boundary result in chatter.
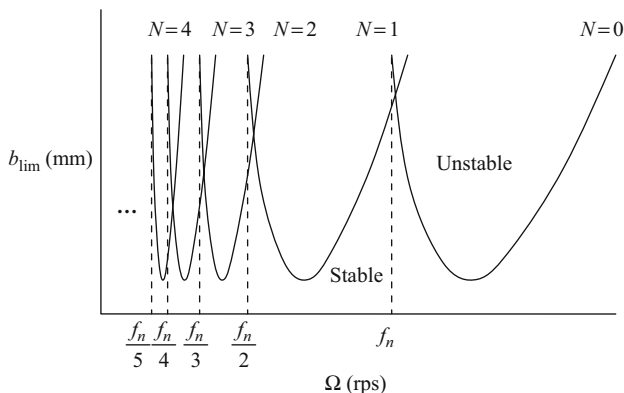

Fig. 3.3.11 Depiction of multiple stability lobes which, taken together, form the stability limit. It is seen that the peaks of the stable zone become less pronounced as N increases

$$\Omega_{best} = \frac{f_n \cdot 60}{N+1} \,(\text{rpm})$$
<div align="right">(3.3.15)</div>

IN A NUTSHELL   We get the same favorable alignment of waviness at many different spindle speeds; these multiple speeds correspond to different numbers of integer waves of vibration imprinted on the workpiece surface per revolution. The increase in allowable chip width without chatter gets larger as the spindle speed gets higher (less waves of vibration per revolution). At lower speeds the lobes overlap to such an extent that the limiting chip width approaches a constant value.

Similarly, we can write a "worst speeds" equation that provides the spindle speeds where the $b_{\text{lim,crit}}$ values are encountered; see Eq. 3.3.16. Equations 3.3.15 and 3.3.16 provide good approximations for dynamic systems that can be modeled as single degree of freedom. Multiple degree of freedom systems, on the other hand, are generally best described using the stability lobe diagram itself.

$$\Omega_{worst} = \frac{f_n(1+\zeta) \cdot 60}{N+\frac{3}{4}} \,(\text{rpm})$$
<div align="right">(3.3.16)</div>

Before discussing the concept of the "oriented FRF" introduced by Tlusty [2], let's take a moment to explore which factors affect b_{lim} and the applicability of stability lobe diagrams to typical turning operations. From Eq. 3.3.1, we see that b_{lim} depends on K_s, β, and the negative real part of the tool point FRF, which we'll describe using the stiffness, k, and damping ratio, ζ. (Again, we are assuming single degree of freedom dynamics.) As K_s and β decrease ($0 \le \beta \le 90\,\text{deg}$), b_{lim} increases. Considering Table 3.1.1, we can see that, all other conditions being equal, we would obtain approximately a three times increase in the allowable chip width if we compared an aluminum alloy with a low alloy steel due to the corresponding K_s values. Considering only the Re[FRF], it becomes less negative as k and ζ are increased (Section 2.2). See the depiction in Fig. 3.3.12, where the increase in k yields not only a less negative real part, but also an increase in the natural frequency. If the workpiece material/tool geometry are unchanged (so that K_s and β can be considered constant), this Re[FRF] change leads to an increase in b_{lim}, but also a shift in the stability lobes. Naturally this would need to be considered in implementation by a spindle speed adjustment.

Example 3.3.1: Best spindle speeds for a single degree of freedom system Let's consider a setup where the tool behaves like a single degree of freedom system with $f_n = 700\,\text{Hz}$ and corresponding k and ζ values determined from a curve
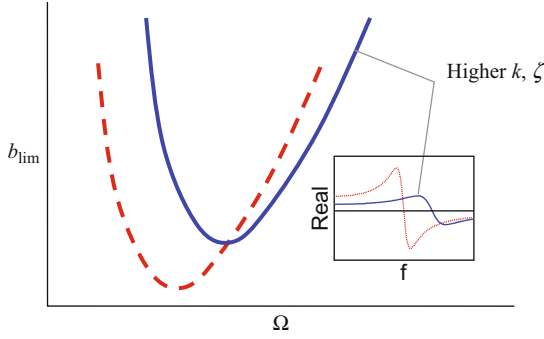
Fig. 3.3.12 Influence of changes in k and ζ on b_{lim}

fit to the direct FRF as measured at the tool point in the y direction. We can apply Eq. 3.3.15 to determine our "best" spindle speed for an increased limiting chip width. If we let $N = 0$ (this gives the right-most peak in the stability lobe diagram), we obtain:

$$\Omega_{best} = \frac{700 \cdot 60}{0 + 1} = 42000 \text{ rpm}.$$

The problem is that conventional lathe spindles don't turn this fast. Let's say the top spindle speed for a selected lathe is 3600 rpm. Which peak, and corresponding best spindle speed, must we then pick? We would require that:

$$\Omega_{best} = \frac{700 \cdot 60}{N + 1} \leq 3600 \text{ rpm}.$$

If we select $N = 11$ (i.e., the 12$^{\text{th}}$ peak counting from right to left in the diagram), the best spindle speed would be 3500 rpm and the maximum spindle speed constraint would be satisfied. However, as seen in Fig. 3.3.11, as N increases the relative improvement in b_{lim} afforded by the stability lobe peaks decreases dramatically. For $N = 11$, the improvement is generally negligible and $b_{\text{lim}} \approx b_{\text{lim,crit}}$. For this reason, stability lobe diagrams are typically more successfully implemented in high speed milling, as opposed to traditional turning operations.

3.4 The Oriented FRF

Using the Tlusty model [2], Eq. 3.3.1 can be rewritten as:

$$b_{\text{lim}} = \frac{-1}{2K_s\mu\text{Re}[FRF]}, \tag{3.4.1}$$

where $\mu = \cos(\beta)$ is referred to as the "directional orientation factor" and the product of μ and Re[FRF] is the real part of the "oriented FRF". The concept is to first project the cutting force, F, into the direction of the system dynamics and, second, project this result into the surface normal, y. The projection into the surface normal is necessary because we are only considering the effects of tool vibrations in this sensitive direction. The two projection steps are required because it may be that the system dynamics are not known in the surface normal direction as we have assumed in our previous descriptions.

Consider, for example, an external turning operation where a square tool bar, whose sides are not aligned with x and y, is used to reduce the diameter of a workpiece; see Fig. 3.4.1. The impact tests described in Section 2.6 would naturally be performed along the tool bar faces (directions u_1 and u_2 in the figure), which would not provide FRFs in the y direction. Here μ would account for these misalignments as well as the force angle and, when combined with the measured FRFs, would provide the system dynamic stiffness in the direction of the surface normal. This is the oriented FRF.
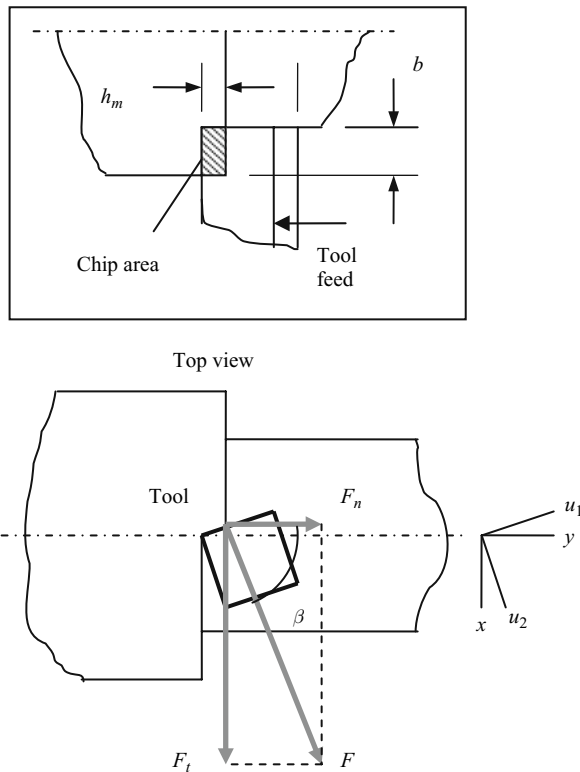

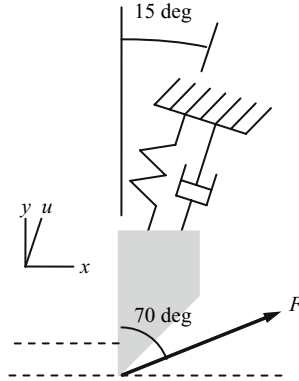Fig. 3.4.1 Oriented FRF description using external turning operation

Fig. 3.4.2 Single degree of freedom system with vibration mode that is not aligned with the surface normal

Example 3.4.1: Single and two degree of freedom oriented FRF   Let's consider an example single degree of freedom system where the vibration mode direction is not aligned with the surface normal as shown in Fig. 3.4.2. In order to calculate the directional orientation factor, the force projection onto the mode direction u is first determined:

$$F_u = F\cos(70 - 15) = F\cos(55).$$

This result is then projected onto the surface normal (y direction).

$$F_n = F_u\cos(15) = F\cos(55)\cos(15)$$

The directional orientation factor is then $\mu = \cos(55)\cos(15) = 0.55$ and the oriented FRF is the product of μ and the FRF measured in the u direction. Because μ is less than one, the oriented FRF appears stiffer than the u direction FRF; see Fig. 3.4.3. Physically, this indicates that only a portion (55%) of the force/flexibility leads to vibration in the sensitive direction.
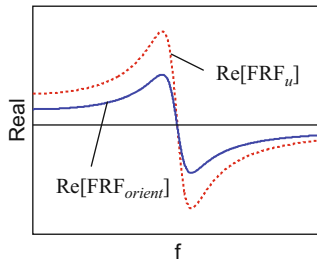

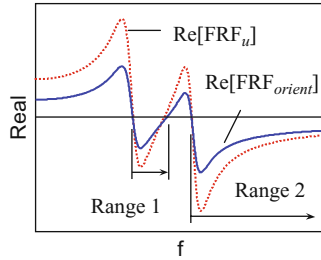**Fig. 3.4.3** Re[FRF] in u direction compared to real part of oriented FRF

Fig. 3.4.4 Re[FRF] in u direction compared to real part of oriented FRF for two degree of freedom system. Two valid chatter frequency ranges are seen

Next, consider the same u direction as shown in Fig. 3.4.2, but now with a second degree of freedom in this direction. The real part of an example two degree of freedom direct FRF at the tool point, as well as the oriented FRF real part, is shown in Fig. 3.4.4. As discussed in Section 3.3, the negative real part is used in the $b_{\lim}$ calculation and defines the valid chatter frequency range. Figure 3.4.4 shows two valid chatter frequency ranges, unlike the previous single degree of freedom examples we've considered. This yields two stability boundary sections for each N value as shown in Ex. 3.4.2.

Example 3.4.2: Competing lobes for two degree of freedom oriented FRF Consider the model shown in Fig. 3.4.5. A two degree of freedom system is aligned with the surface normal and the force angle is 70 deg. The directional orientation factor therefore only requires the projection of the force into the mode
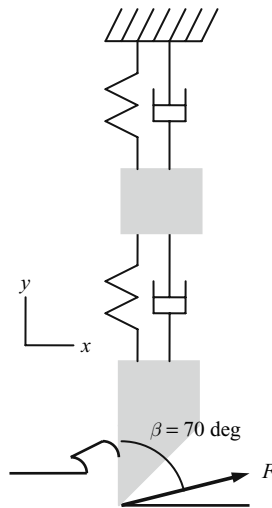

Fig. 3.4.5 Two degree of freedom model for turning stability evaluation
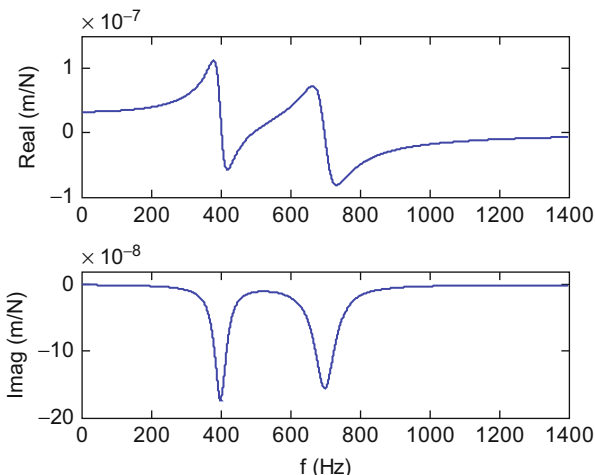
Fig. 3.4.6 Real and imaginary parts of the oriented FRF for the system in Ex. 3.4.2

direction, $\mu = \cos(70)$.   The   modal   parameters   are: $f_{n1} = 400\,\text{Hz}$, $k_{q1} = 2 \times 10^7\,\text{N/m}$, $\zeta_{q1} = 0.05$, $f_{n2} = 700\,\text{Hz}$, $k_{q2} = 2.2 \times 10^7\,\text{N/m}$,,   and $\zeta_{q2} = 0.05$. We will determine the stability behavior for this turning operation.

The real and imaginary parts of the oriented FRF for this system are shown in Fig. 3.4.6. Two distinct modes with 400 Hz and 700 Hz natural frequencies are observed. As seen previously in Fig. 3.4.4, there are two valid chatter frequency ranges associated with this two mode system. They occur where the real part is less than zero and are pictured in the top panel of Fig. 3.4.7. In the
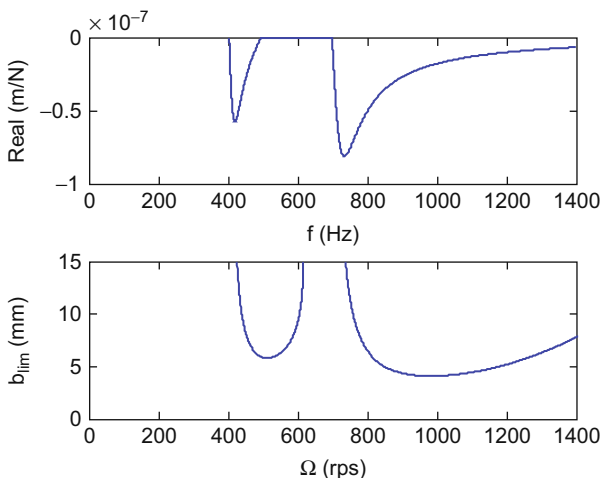

Fig. 3.4.7 (Top panel) Negative real part of oriented FRF. (Bottom panel) Corresponding $N = 0$ stability limit. The two lobes sections are present due to the two portions of the negative real part in the top panel

bottom panel, the Ω and b_{lim} values, which are both a function of the FRF and therefore the chatter frequency (as seen in Eqs. 3.1–3.3), are plotted against one another to define the stability limit ($K_s = 1500$ N/mm^2). It is seen that a distinct lobe section is associated with each of the two chatter frequency ranges. Only the $N = 0$ pair is shown in this figure. However, it is the whole family of curves, $N = 0, 1, 2, \ldots$, that defines the overall stability boundary. The $N = 0, 1,$ and 2 lobes are shown in Figure 3.4.8. Because these lobes can interfere with each other and limit the stable chip width, they may be considered as "competing lobes". For example, it is seen that the right portion of the $N = 2$ lobe (corresponding to the 700 Hz mode) truncates the stable zone between the left (400 Hz mode) and right portions of the $N = 1$ lobe near 20000 rpm. The MATLAB® program used to produce these figures is provided on the companion CD as p_3_4_2_1.m.

As seen in Figure 3.4.1, it is sometimes not sufficient to consider the system flexibility in one direction only. In this case, modes in both the u_1 and u_2 directions should be included in the stability evaluation described in the previous example. The model shown in Fig. 3.4.9 depicts a single degree of freedom aligned with both u_1 and u_2, neither of which are coincident with y, the surface normal. The oriented FRF now depends on the contributions of both modes. We therefore calculate two directional orientation factors, each of which projects the force into the appropriate mode and then this result into the surface normal. Let's consider the u_1 mode. The first step is to project F into the u_1 direction:

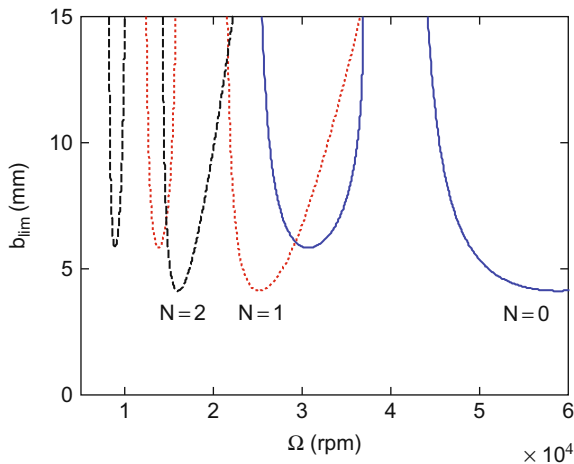$$F_{u_1} = F\cos(\beta - \alpha_1). \tag{3.4.2}$$

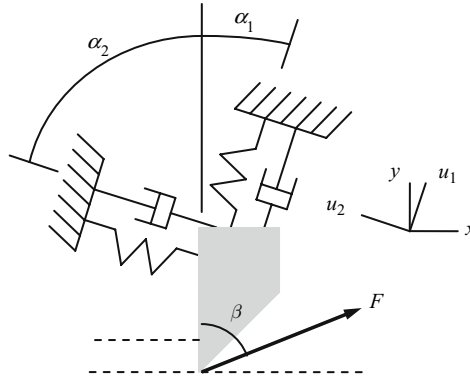Fig. 3.4.8 Competing $N = 0, 1,$ and 2 stability lobes for two degree of freedom system

Fig. 3.4.9 Turning model with a single degree of freedom in both the u_1 and u_2 directions

This result is then projected into the surface normal:

$$F_n = F_{u_1} \cos(\alpha_1) = F\cos(\beta - \alpha_1) \cos(\alpha_1). \qquad (3.4.3)$$

The u_1 directional orientation factor is, therefore, $\mu_1 = \cos(\beta - \alpha_1) \cos(\alpha_1)$. Similarly, the steps in determining μ_2 are:

$$F_{u_2} = F\cos(\beta + \alpha_2) \text{ and} \qquad (3.4.4)$$

$$F_n = F_{u_{12}} \cos(\alpha_2) = F\cos(\beta + \alpha_2) \cos(\alpha_2) \qquad (3.4.5)$$

so that $\mu_2 = \cos(\beta + \alpha_2) \cos(\alpha_2)$. The oriented FRF is then calculated as a linear combination of the contributions of both modes/cutting force using these directional orientation factors. Note that this treatment is not limited to a single degree of freedom in either direction; it is generic to any number of degrees of freedom in the two perpendicular directions u_1 and u_2.

$$FRF_{orient} = \mu_1 FRF_{u_1} + \mu_2 FRF_{u_2} \qquad (3.4.6)$$

IN A NUTSHELL   It is possible for a multiple degree of freedom system to chatter in any of its modes. The effect of each mode is determined by its dynamic characteristics, the alignment of the force with the direction of flexibility of the mode, and the ability of the deflection of the mode to imprint on the surface of the workpiece. These effects are combined in the "directional orientation factor".

Example 3.4.3: Turning model with modes in two perpendicular directions We'll next determine the stability for the model in Fig. 3.4.9 with the following parameters: $\alpha_1 = 30$ deg, $\alpha_2 = 60$ deg, $\beta = 70$ deg, and $K_s = 2000$ N/mm^2. The dynamics are defined by $f_{n1} = 421$ Hz,, $k_1 = 2.8 \times 10^7$ N/m, and, and $\zeta_1 = 0.05$ for the u_1 direction and $f_{n2} = 491$ Hz,, $k_2 = 3.81 \times 10^7$ N/m, and $\zeta_2 = 0.05$ for the u_2 direction. The directional orientation factors are calculated using Eqs. 3.4.2–3.4.5.

$$\mu_1 = \cos(\beta - \alpha_1)\cos(\alpha_1) = \cos(70 - 30)\cos(30) = 0.663$$

$$\mu_2 = \cos(\beta + \alpha_2)\cos(\alpha_2) = \cos(70 + 60)\cos(60) = -0.321$$

The oriented FRF, as well as its components $\mu_1 FRF_{u_1}$ and $\mu_2 FRF_{u_2}$, are shown in Fig. 3.4.10. It is seen that: 1) the minimum real part of FRF_{orient} occurs at 443 Hz with a value of 1.493×10^{-4} mm/N; and 2) the real part crosses through zero amplitude at a frequency of 418 Hz (which corresponds to the natural frequency for a single degree of freedom system). Although this is not a single degree of freedom system, the real part of the oriented FRF bears some similarity to a single degree of freedom FRF real part. As an approximation, we can therefore calculate $b_{\mathrm{lim,crit}}$ and the best and worst spindle speeds using the single degree of freedom equations presented in Section 3.3. The best and worst spindle speeds are summarized in Table 3.4.1.
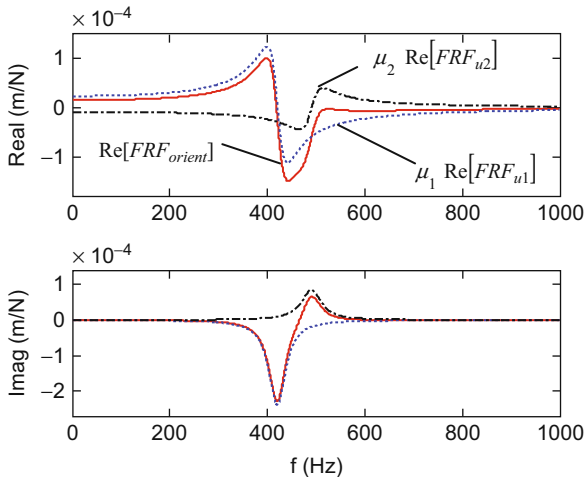

Fig. 3.4.10 Oriented FRF for Ex. 3.4.2. The two components of the oriented FRF are also shown

Table 3.4.1 Approximate best and worst spindle speeds for Ex. 3.4.2

N	Ω_{best} (rps)	Ω_{best} (rpm)	Ω_{worst} (rps)	Ω_{worst} (rpm)
0	418	25080	591	35460
1	209	12540	253	15180
2	139	8340	161	9665
3	105	6300	118	7088

$$b_{\text{lim,crit}} = \frac{-1}{2K_s \cdot \min(\text{Re}[FRF_{orient}])} = \frac{-1}{2 \cdot 2000 \cdot (-1.493 \times 10^{-4})} = 1.7\,\text{mm}$$

$$\Omega_{best} = \frac{418}{N+1}\,(\text{rps})$$

$$\Omega_{worst} = \frac{443}{N+\frac{3}{4}}\,(\text{rps})$$

Figure 3.4.11 shows one valid chatter frequency range associated with the oriented FRF. As before, it occurs where the real part is less than zero (top panel). In the bottom panel, the $N = 0$ Ω and b_{lim} values are plotted against one another to define the stability limit. It is seen that the best speed of 418 rps is a reasonable approximation of the actual behavior. Figure 3.4.12 shows the combined stability boundary for $N = 0$ to 3. The MATLAB® program used to produce these figures is provided on the companion CD as p_3_4_3_1.m. Note that ε in Eq. 3.3.3 must now be calculated using FRF_{orient}.
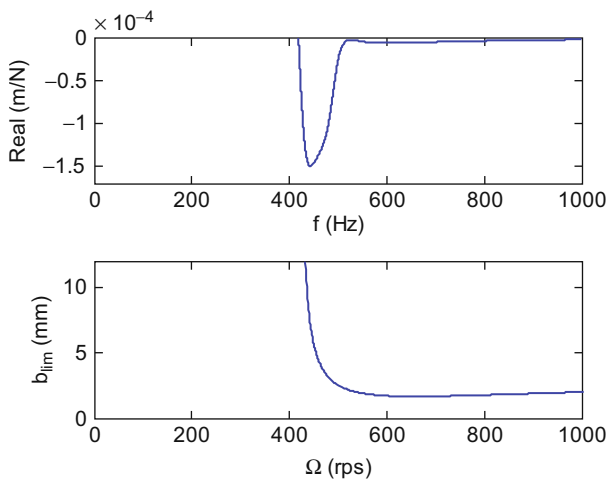

Fig. 3.4.11 (Top panel) Negative real part of oriented FRF for Ex. 3.4.3. (Bottom panel) Corresponding $N = 0$ stability limit
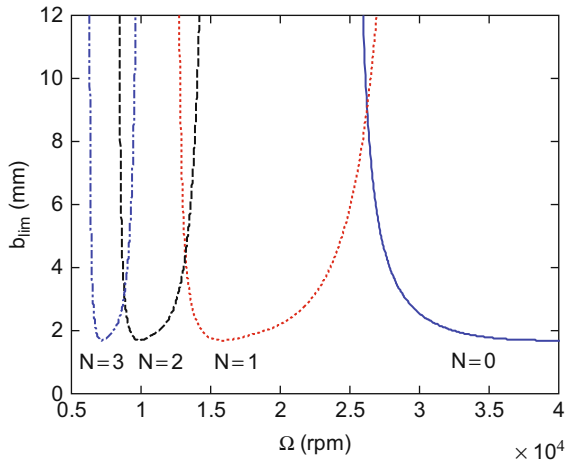
Fig. 3.4.12 Stability lobes for Ex. 3.4.3 ($N = 0$ to 3)

3.5 Turning Time-Domain Simulation

In this section, a time-domain simulation is described that solves the turning equation of motion by numerical integration. This is in contrast to Tlusty's analytical, frequency-domain solution detailed in the previous sections. The stability lobe diagram determined from the analytical solution gives a "global" picture of the stability behavior for a particular turning setup, but does not provide information regarding the cutting force or tool vibrations. On the other hand, time-domain simulation gives "local" force and vibration levels for the selected cutting conditions, but not the same global view. The simulation proceeds as follows: 1) the instantaneous chip thickness is determined using the current and previous tool vibrations; 2) the cutting force is calculated; 3) the force is used to find the new displacement; and 4) the process is repeated in small time steps. The simulation model is the same as was presented in Fig. 3.4.9.

3.5.1 Chip Thickness Calculation

As shown in Eq. 3.2.1, the instantaneous chip thickness depends, at minimum, on the mean chip thickness (or feed per revolution), the current normal (y) direction vibration, and the vibration one revolution earlier, $h(t) = h_m + y(t - \tau) - y(t)$. We used Fig. 3.2.3 as an aid in visualizing this equation. In reality, the situation is a little more complicated because, depending on the vibration levels, the instantaneous chip thickness may depend on the current vibration and the vibration two revolutions earlier, for example. Consider the vibrations in two subsequent
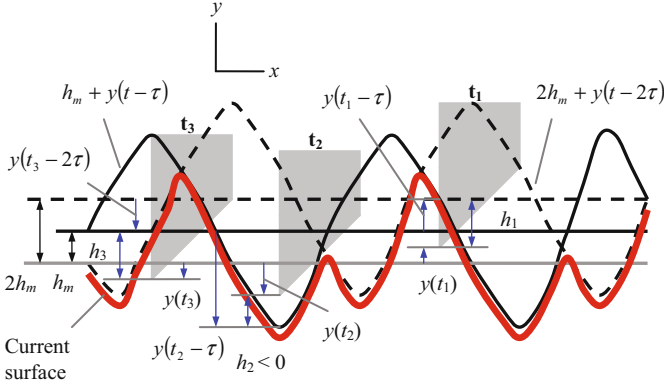
Fig. 3.5.1 Chip thickness determination at three different instants in time

revolutions shown in Fig. 3.5.1. The current vibration state is defined by the tool position at three different times, t_1, t_2, and t_3. The vibration one revolution earlier is represented by the solid, sinusoidal line and is offset from the current commanded mean chip thickness line by h_m. The vibration two revolutions earlier is shown as a dashed line and is offset by $2h_m$. The current surface is given by the heavy solid line. It is seen that the current surface depends on the previous revolution at certain times (including t_1 and t_2) and the vibration two revolutions earlier at other times (such as t_3). At t_1, the chip thickness is determined in the traditional manner, $h_1 = h_m + y(t_1 - \tau) - y(t_1)$. At t_2, the tool point is actually above the current surface. In other words, no cutting is taking place. Here, $h_3 = 2h_m + y(t_3 - 2\tau) - y(t_3)$ so that $h_2 < 0$. Clearly, a negative chip thickness does not make physical sense, but this nonlinearity is conveniently incorporated in the simulation. At t_3, the chip thickness is determined using $h_3 = 2h_m + y(t_3 - 2\tau) - y(t_3)$ At this instant, we must consider the vibrations two revolutions prior.

The simulation is carried out in small time steps, dt. Because we are numerically integrating the system equation of motion to determine the tool vibrations, care must be exercised in selecting dt. If the value is too large, inaccurate results are obtained. As a rule of thumb, it is generally acceptable to set dt at least 10 times smaller than the period corresponding to the highest natural frequency in the system's dynamic model.

Example 3.5.1: Numerical integration time step selection Consider a turning model with two natural frequencies, $f_{n1} = 800$ Hz and $f_{n2} = 1000$ Hz. The period of the higher natural frequency is:

$$\tau_2 = \frac{1}{f_{n2}} = 1 \times 10^{-3}\,\text{s}$$

and the maximum dt value should be:

$$dt = \frac{\tau_2}{10} = 1 \times 10^{-4} \text{ s.}$$

Smaller values are naturally acceptable (dividing the time constant by 50 or 100, for example), but there is a tradeoff between improved numerical accuracy and execution time for the simulation.

Once the time step is selected, the simulation time can be determined using:

$$t_n = n \cdot dt, \tag{3.5.1}$$

where n is the simulation counter ($n = 1, 2, \ldots$). The number of time steps per spindle revolution, or *steps_rev*, is related to dt (in sec) and the selected spindle speed, Ω (in rpm), as:

$$steps\_rev = \frac{60}{dt \cdot \Omega}. \tag{3.5.2}$$

This value is critical because it enables us to keep track of the vibration state from one revolution to the next. At some discrete time t_n in the simulation, the behavior one revolution earlier ($t - \tau$ in a continuous sense) is $t_{n-steps\_rev}$ (in a discrete sense). In practice, because *steps_rev* is used as part of the index for the simulation variables, only integer values are allowed. This is accomplished in MATLAB® using the round function. For example:

```
steps_rev= round(60/(dt*omega));
```

where omega represents the spindle speed in rpm. In simulation, the dependence of the actual surface on more than the most previous revolution can be incorporated by calculating the chip thickness according to:

$$h = y_{\min} - y_{n-1}, \tag{3.5.3}$$

where $y_{\min}$ is the smallest value of $\{\{h_m + y_{n-steps\_rev}, 2h_m + y_{n-2\cdot steps\_rev}, \ldots\}$ which, according to Fig. 3.5.1, defines the current workpiece surface. The index (n-1) on y in Eq. 3.5.3 is used because the vibration in the current time step (with index n) is only known after the force is determined and the equation of motion is solved.

3.5.2 Force Calculation

Once the chip thickness is computed using Eq. 3.5.3, the force in the current time step is determined using the selected chip width, b, and specific force:

$$F = K_s bh. \tag{3.5.4}$$

As described previously, it is possible that the calculated chip thickness will be negative if the current tool vibration is larger than the surface location (refer to Fig. 3.5.1 at t_2). In this case, no cutting is occurring. Therefore, the cutting force should be zero. We incorporate this nonlinearity by setting the force equal to zero if the result from Eq. 3.5.4 is less than zero (due to a negative chip thickness). Additionally, the surface is updated to reflect the actual location, y_{min}, rather than the tool vibration: $y_{n-1} = y_{min}$ Once the cutting force is known, it is resolved into the mode directions, u_1 and u_2, as depicted in Fig. 3.4.9.

$$F_{u_1} = F\cos(\beta - \alpha_1) \text{ and } F_{u_2} = F\cos(\beta + \alpha_2) \qquad (3.5.5)$$

3.5.3 Displacement Calculation

Considering the single degree of freedom models shown in the u_1 and u_2 directions in Fig. 3.4.9, the corresponding equations of motion are:

$$m_1\ddot{u}_1 + c_1\dot{u}_1 + k_1u_1 = F_{u_1} \text{ and } m_2\ddot{u}_2 + c_2\dot{u}_2 + k_2u_2 = F_{u_2}. \qquad (3.5.6)$$

The mode direction accelerations in the current time step due to the two force components are determined by rewriting Eq. 3.5.6:

$$\ddot{u}_1 = \frac{F_{u_1} - c_1\dot{u}_1 + k_1u_1}{m_1} \text{ and } \ddot{u}_2 = \frac{F_{u_2} - c_2\dot{u}_2 + k_2u_2}{m_2}, \qquad (3.5.7)$$

where the velocities, $\dot{u}_1$ and $\dot{u}_2$, and positions, u_1 and u_2, from the previous time step are used (they are set equal to zero initially). The velocities and positions for the current time step are then determined by numerical (Euler) integration:

$$\dot{u}_1 = \dot{u}_1 + \ddot{u}_1 dt \text{ and } \dot{u}_2 = \dot{u}_2 + \ddot{u}_2 dt \qquad (3.5.8)$$

$$u_1 = u_1 + \dot{u}_1 dt \text{ and } u_2 = u_2 + \dot{u}_2 dt, \qquad (3.5.9)$$

where the velocities on the right hand side of the equal signs in Eq. 3.5.8 are retained from the previous time step and used to update the current values. These current values are then applied to determine the current displacements in Eq. 3.5.9. Again, the displacements on the right hand side of Eq. 3.5.9 are those from the previous time step. Once u_1 and u_2 are known, they are projected into the normal (y) direction:

$$y_n = u_1\cos(\alpha_1) + u_2\cos(\alpha_2), \qquad (3.5.10)$$

where the n subscript on y indicates the time step. Note that this value represents y_{n-1} in the next time step and is applied in Eq. 3.5.3 to calculate the updated chip

thickness. The process of computing the force and resulting displacements is then repeated.

Example 3.5.2: Stability evaluation by time-domain simulation Consider the turning model shown in Fig. 3.5.2. The dynamic constants are: $m_1 = 1\,\mathrm{kg}$, $c_1 = 450\,\mathrm{N-s/m}$, and $k_1 = 2 \times 10^7\,\mathrm{N/m}$ for the u_1 direction and $m_2 = 1\,\mathrm{kg}$, $c_2 = 650\,\mathrm{N-s/m}$, and $k_2 = 3 \times 10^7\,\mathrm{N/m}$ for the u_2 direction. The other parameters are: $\alpha_1 = 35\,\mathrm{deg}$, $\alpha_2 = 55\,\mathrm{deg}$, $\beta = 65\,\mathrm{deg}$, $h_m = 0.1\,\mathrm{mm}$, and $K_s = 2000\,\mathrm{N/mm}^2$. Prior to determining the time-domain force and displacements using the simulation described in the previous paragraphs, let's calculate $b_{\mathrm{lim,crit}}$, the approximate best and worst speeds, and the stability lobe diagram for this model.

As seen in Ex. 3.4.3, the oriented FRF must be determined using the directional orientation factors prior to calculating $b_{\mathrm{lim,crit}}$. The directional orientation factors are:

$$\mu_1 = \cos(\beta - \alpha_1)\cos(\alpha_1) = \cos(65 - 35)\cos(35) = 0.709 \text{ and}$$

$$\mu_2 = \cos(\beta + \alpha_2)\cos(\alpha_2) = \cos(65 + 55)\cos(55) = -0.287.$$

The oriented FRF is displayed in Fig. 3.5.3. The minimum real part of occurs at 748 Hz with a value of $1.993 \times 10^{-4}\,\mathrm{mm/N}$ and the real part crosses through zero amplitude at a frequency of 709 Hz. Similar to Ex. 3.4.3, although this is not a single degree of freedom system, the real part of the oriented FRF resembles single degree of freedom system behavior. We can therefore approximate $b_{\mathrm{lim,crit}}$ and the best and worst spindle speeds using the single degree of freedom equations presented in Section 3.3. The best and worst spindle speeds are summarized in Table 3.5.1.
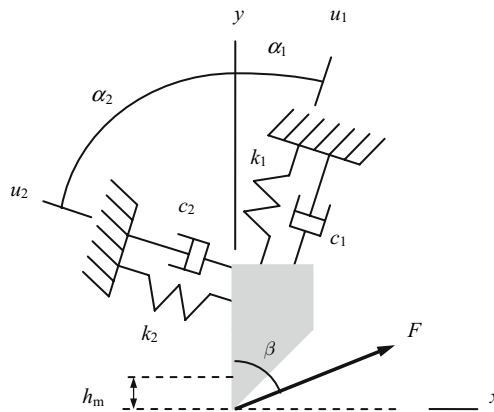

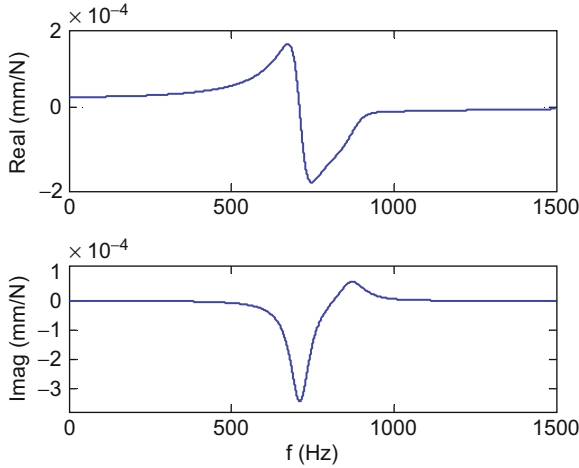**Fig. 3.5.2** Model for turning time-domain simulation in Ex. 3.5.2

Fig. 3.5.3 Oriented FRF for Ex. 3.5.2

$$b_{\lim,\text{crit}} = \frac{-1}{2K_s \cdot \min(\text{Re}[FRF_{orient}])} = \frac{-1}{2 \cdot 2000 \cdot (-1.993 \times 10^{-4})} = 1.3 \, \text{mm}$$

$$\Omega_{best} = \frac{709}{N+1} \, (\text{rps})$$

$$\Omega_{worst} = \frac{748}{N+\frac{3}{4}} \, (\text{rps})$$

The top panel of Fig. 3.5.4 shows a single valid chatter frequency range (real part < 0) for the oriented FRF. In the bottom panel, it is observed that the best speed of 709 rps is an acceptable approximation of the actual behavior, although this is not a reasonable spindle speed (42540 rpm) for typical turning applications. Figure 3.5.5 shows the combined stability boundary for $N = 0$ to 4. The MATLAB® programs used to produce these figures are provided on the companion CD as p_3_5_2_1.m and p_3_5_2_2.m.

As discussed before, Fig. 3.5.5 provides a global view of the process stability, but does not provide local information, such as force and tool displacement,

Table 3.5.1 Approximate best and worst spindle speeds for Ex. 3.5.2

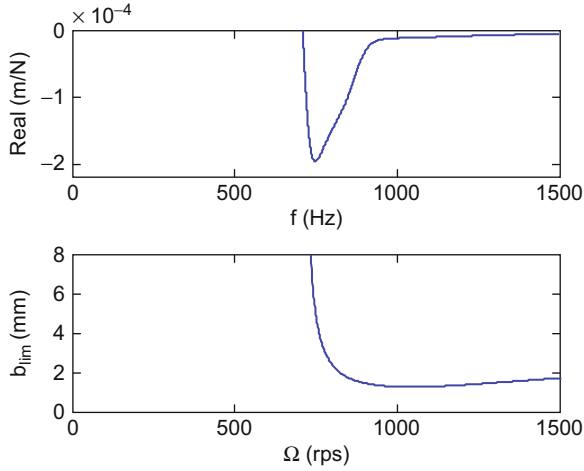| N	Ω_{best} (rps)	Ω_{best} (rpm)	Ω_{worst} (rps)	Ω_{worst} (rpm)
0	709	42540	997	59840
1	355	21270	427	25646
2	236	14180	272	16320
3	177	10635	199	11968
4	142	8508	157	9448

Fig. 3.5.4 (Top panel) Negative real part of oriented FRF for Ex. 3.5.2. (Bottom panel) Corresponding $N = 0$ stability limit
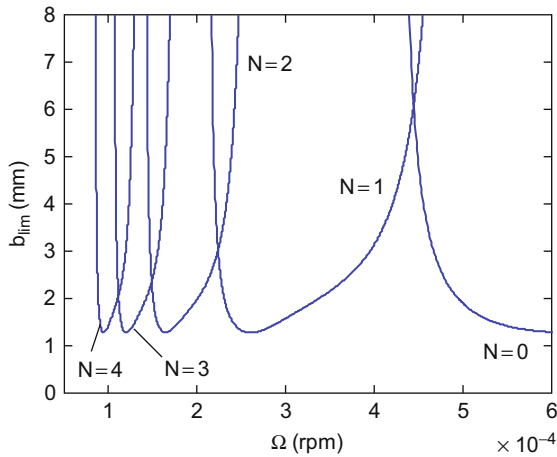

Fig. 3.5.5 Stability lobes for Ex. 3.5.2 ($N = 0$ to 4)

about particular operating parameter combinations. For example, the stability boundary would suggest that 44490 rpm is a good operating speed for b values up to 6 mm [this spindle speed is somewhat higher than the simple approximation of 42540 rpm provided in Table 3.5.1]. It also shows that the maximum allowable chip width at 26140 rpm is slightly less than 1.3 mm. We will now use the time-domain simulation to determine the force and tool displacement values near these stability thresholds. Figure 3.5.6 provides the results for $\Omega = 44490$ rpm and $b = 5$ mm, where the total simulation time
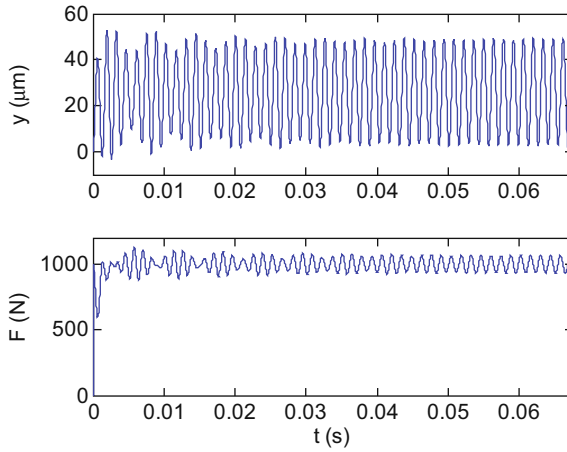
Fig. 3.5.6 Example 3.5.2 time-domain force and displacement for $\Omega = 44490$ rpm and $b = 5$ mm

corresponds to 50 revolutions, $\frac{50}{\frac{44490}{60}} = 0.067$s. It is seen that these conditions are actually near the stability limit since the force and displacement levels are neither growing nor diminishing. In this way, time-domain simulation can be used to refine the analytical stability limit results. We can also check the simulation mean values against Eqs. 3.5.11 and 3.5.12. Equation 3.5.11 gives the mean cutting force, F_m, based on the commanded chip area and specific force. Equation 3.5.12 provides the mean normal direction displacement, y_m, where the sum of the $\frac{\mu}{k}$ ratios gives the static compliance of the oriented FRF. As expected, the simulation results in Fig. 3.5.6 agree with the analytical expressions in both cases. At $\Omega = 44490$ rpm and $b = 6$ mm, the cut is clearly unstable; the force and displacement values are growing significantly with time. See Fig. 3.5.7.

$$F_m = K_s b h_m = 2000 \cdot 5 \cdot 0.1 = 1000 \,\text{N} \tag{3.5.11}$$

$$y_m = F_m \left(\frac{\mu_1}{k_1} + \frac{\mu_2}{k_2} \right) = 1000 \left(\frac{0.709}{2 \times 10^7} + \frac{-0.287}{3 \times 10^7} \right) = 2.6 \times 10^{-5} \,\text{m} = 26 \,\mu\text{m} \tag{3.5.12}$$

At the less favorable spindle speed of $\Omega = 26140$ rpm, chatter is observed at $b = 2$ mm in Fig. 3.5.8. Not only are the force and displacement values growing with time, but the force nonlinearity is also observed (beginning at approximately $t = 0.025$ s) when the tool vibration grows large enough that there is no cutting intermittently and $F = 0$. The total simulated time for 50 revolutions is now: $\frac{50}{\frac{26140}{60}} = 0.067$s. If the chip width is reduced to 1 mm, stable operation is obtained (Fig. 3.5.9). Here it is seen that the initial transient response quickly
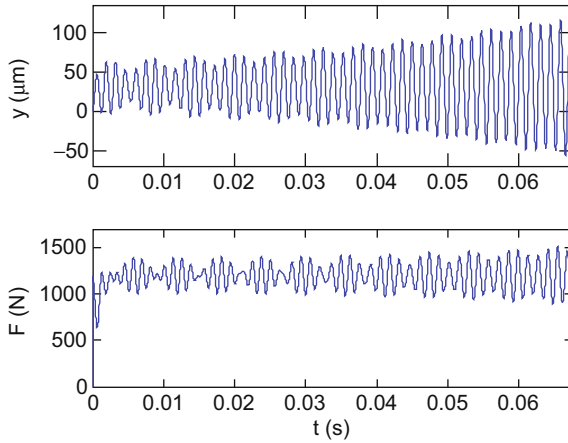
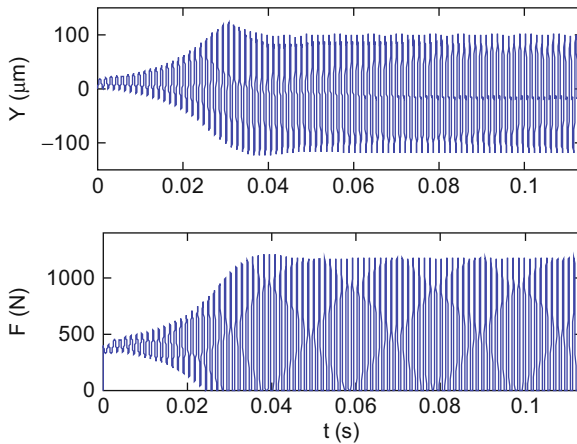**Fig. 3.5.7** Example 3.5.2 time-domain force and displacement for $\Omega = 44490$ rpm and $b = 6$ mm

Fig. 3.5.8 Example 3.5.2 time-domain force and displacement for $\Omega = 26140$ rpm and $b = 2$ mm

attenuates and the steady state force and displacement are obtained. The MATLAB® program used to produce these figures is provided on the companion CD as p_3_5_2_3.m.

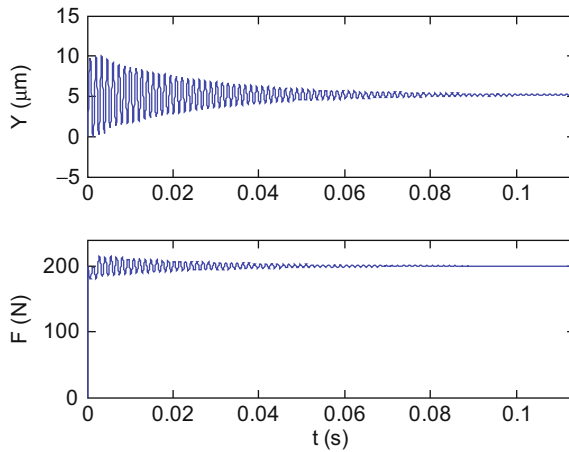$$F_m = K_s b h_m = 2000 \cdot 1 \cdot 0.1 = 200 \, \text{N}$$

Fig. 3.5.9 Example 3.5.2 time-domain force and displacement for $\Omega = 26140$ rpm and $b = 1$ mm

$$y_m = F_m \left(\frac{\mu_1}{k_1} + \frac{\mu_2}{k_2} \right) = 200 \left(\frac{0.709}{2 \times 10^7} + \frac{-0.287}{3 \times 10^7} \right) = 5 \times 10^{-6} \, \text{m} = 5 \, \mu\text{m}$$

IN A NUTSHELL   Time-domain simulation eliminates many of the simplifying assumptions required to obtain the global analytical solution. For that reason, time-domain simulation is more accurate than the analytical solution. However, it provides information on a case-by-case basis only. Using time-domain simulation to produce a stability lobe diagram requires many repeated executions.

3.5.4 Multiple Degree of Freedom Modeling

As a final point of consideration in this section, let's discuss how to extend the time-domain simulation to include multiple degrees of freedom in the two mode directions u_1 and u_2. The important point to remember from Chapter 2 is that, provided we have measured the direct FRF at the location of interest (the tool point), the response can be expressed as a sum of the modal contributions. Therefore, once we have completed the curve fitting exercise to obtain the modal parameters (Section 2.5), we can treat each degree of freedom for both mode directions separately and determine the individual solutions using Euler integration as shown in Eqs. 3.5.7 through 3.5.9. After the displacements in each mode have been calculated, they are simply summed in each direction. For example, assume that two modes were identified and curve fitted using peak

picking for the u_1 direction and three modes were selected for the u_2 direction. The modal parameters m_{q1,u_1}, c_{q1,u_1}, k_{q1,u_1}, m_{q2,u_1}, c_{q2,u_1}, and k_{q2,u_1} would be obtained for u_1, while m_{q1,u_2}, c_{q1,u_2}, k_{q1,u_2}, m_{q2,u_2}, c_{q2,u_2}, k_{q2,u_2}, m_{q3,u_2}, c_{q3,u_2}, and k_{q3,u_2} would be obtained for u_2. The modal accelerations in the u_1 direction would now include:

$$\ddot{u}_{1,q1} = \frac{F_{u_1} - c_{q1,u_1}\dot{u}_{1,q1} + k_{q1,u_1}u_{1,q1}}{m_{q1,u_1}} \text{ and } \ddot{u}_{1,q2} = \frac{F_{u_1} - c_{q2,u_1}\dot{u}_{1,q2} + k_{q2,u_1}u_{1,q2}}{m_{q2,u_1}},$$

where the local u_1 direction force is used because the modal force vector is composed of identical local force values for each modeled mode (see Eq. 2.4.4.). The modal coordinate velocities and positions would then be determined according to:

$$\dot{u}_{1,q1} = \dot{u}_{1,q1} + \ddot{u}_{1,q1}dt \quad \text{and} \quad \dot{u}_{1,q2} = \dot{u}_{1,q2} + \ddot{u}_{1,q2}dt \quad \text{and}$$

$$u_{1,q1} = u_{1,q1} + \dot{u}_{1,q1}dt \quad \text{and} \quad u_{1,q2} = u_{1,q2} + \dot{u}_{1,q2}dt.$$

Finally, the u_1 local displacement would be calculated using: $u_1 = u_{1,q1} + u_{1,q2}$. Similarly, the u_2 direction modal accelerations would be:

$$\ddot{u}_{2,q1} = \frac{F_{u_2} - c_{q1,u_2}\dot{u}_{2,q1} + k_{q1,u_2}u_{2,q1}}{m_{q1,u_2}}, \ddot{u}_{2,q2} = \frac{F_{u_2} - c_{q2,u_2}\dot{u}_{2,q2} + k_{q2,u_2}u_{2,q2}}{m_{q2,u_2}}, \text{and}$$

$$\ddot{u}_{2,q3} = \frac{F_{u_2} - c_{q3,u_2}\dot{u}_{2,q3} + k_{q3,u_2}u_{2,q3}}{m_{q3,u_2}}.$$

The modal coordinate velocities and positions in the u_2 direction would then be determined using:

$$\dot{u}_{2,q1} = \dot{u}_{2,q1} + \ddot{u}_{2,q1}dt, \dot{u}_{2,q2} = \dot{u}_{2,q2} + \ddot{u}_{2,q2}dt, \quad \text{and} \quad \dot{u}_{2,q3} = \dot{u}_{2,q3} + \ddot{u}_{2,q3}dt$$

$$u_{2,q1} = u_{2,q1} + \dot{u}_{2,q1}dt u_{2,q2} = u_{2,q2} + \dot{u}_{2,q2}dt \quad \text{and} \quad u_{2,q3} = u_{2,q3} + \dot{u}_{2,q3}dt$$

and the u_2 local displacement would be calculated using: $u_2 = u_{2,q1} + u_{2,q2} + u_{2,q3}$. As with the single degree of freedom case, all initial values of the modal velocities and displacements should be set equal to zero prior to simulation execution.

IN A NUTSHELL   Modal analysis provides a convenient way to summarize the dynamic characteristics of complicated vibration systems. When applying time-domain simulation, the compact modal data representation facilitates determination of the appropriate parameters for stable machining.

Exercises

1. For the turning schematic shown in Fig. e.3.1., complete parts a) through f). For the single degree of freedom dynamics, the mass is 2 kg, the damping ratio is 0.05, and the stiffness is 2×10^7 N/m. The u direction is oriented at an angle, α, of 35 deg relative to the surface normal, y. The force model parameters are $K_s = 1500$ N/mm^2 and $\beta = 70$ deg.
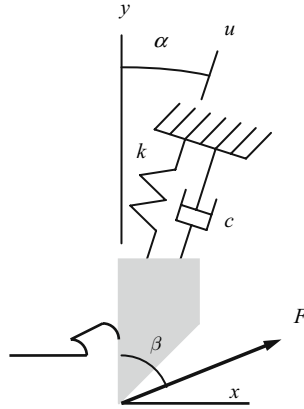

Fig. e.3.1 Turning model with flexible tool

   a) Calculate the directional orientation factor. Using this value, compute and plot the real and imaginary parts (in m/N) of the oriented frequency response function vs. frequency (in Hz).
   b) Determine the minimum value of the real part of the oriented frequency response function and the corresponding chatter frequency. Calculate $b_{\text{lim,crit}}$.
   c) Determine the spindle speed (in rpm) corresponding to the stability peak defined by the intersection of the $N = 0$ and $N = 1$ stability lobes.
   d) Find the spindle speed (in rpm) corresponding to the minimum stability limit for the $N = 0$ lobe.
   e) Determine the spindle speed (in rpm) corresponding to the stability peak defined by the intersection of the $N = 3$ and $N = 4$ stability lobes.
   f) Plot the first four stability lobes ($N = 0$ to 3) for this system. Use b_{lim} units of mm and spindle speed units of rpm.

2. Using the turning schematic shown in Fig. e.3.2., complete parts a) through d). For the u_1 direction, the mass is 10 kg, the damping is 170 N-s/m, and the stiffness is 7×10^6 N/m. The u_1 direction is oriented at an angle, α_1, of 60 deg relative to the surface normal, y. For the u_2 direction, the mass is 12 kg, the damping is 1700 N-s/m, and the stiffness is 5×10^7 N/m. The u_2 direction is oriented at an angle, α_2, of 30 deg relative to the y direction. The force model parameters are $K_s = 2000$ N/mm^2 and $\beta = 60$ deg.
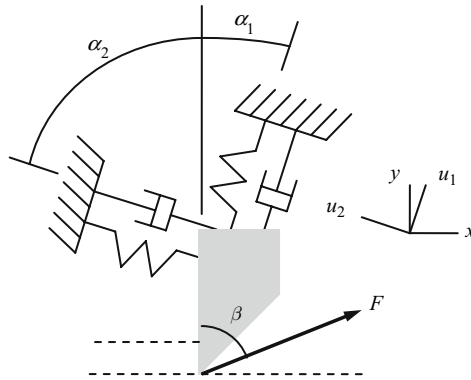
Fig. e.3.2 Turning model with a single degree of freedom in both the u_1 and u_2 directions

a) Compute the directional orientation factors, μ_1 and μ_2. Plot the real and imaginary parts (in m/N) of the oriented frequency response function vs. frequency (in Hz).

b) Determine the minimum value of the real part of the oriented frequency response function and the corresponding chatter frequency. Calculate $b_{lim,crit}$.

c) Find the spindle speed (in rpm) corresponding to the minimum stability limit for the $N = 2$ lobe.

d) Plot the first five stability lobes ($N = 0$ to 4) for this system. Use b_{lim} units of mm and spindle speed units of rpm.

3. Considering the turning model shown in Fig. e.3.3, determine the critical stability limit if $K_s = 750$ N/mm^2. For both lumped parameter degrees of freedom, the mass is 1 kg, the stiffness is 7×10^6 N/m, and the damping is 200 N-s/m.
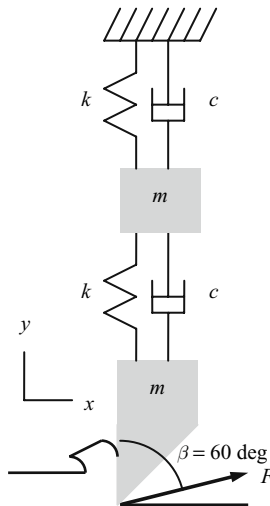

Fig. e.3.3 Two degree of freedom turning model

4. Complete time-domain simulations for the turning model described in
   Exercise 2. Evaluate the following points for stable or unstable behavior.
   Use a mean chip thickness (feed per revolution) of 0.15 mm and carry out
   your simulations for 25 revolutions.

Ω (rpm)	b (mm)
2150	0.1
2150	0.5
2500	0.1
2500	0.5
2930	0.1
2930	0.5
3750	0.1
3750	0.5
4600	0.1
4600	0.5

Superimpose your results on the stability lobe diagram from Exercise 2,
part d). Use a circle for stable operating points and an 'x' for unstable points.

References

1. Trent, E. and Wright, P., 2000, Metal Cutting, 4th Ed., Butterworth-Heinemann, Boston,
   MA.
2. Tlusty, G., 2000, Manufacturing Equipment and Processes, Prentice-Hall, Upper Saddle
   River, NJ.
3. Altintas, Y., 2000, Manufacturing Automation: Metal Cutting Mechanics, Machine Tool
   Vibrations, and CNC Design, Cambridge University Press, Cambridge.
4. Stephenson, D. and Agapiou, J., 1997, Metal Cutting Theory and Practice, Marcel
   Dekker, Inc., New York, NY.